

Application and Performance Assessment of Annealing Methods for Electrostatic-Energy-Based Configuration Search in Mixed Crystals*

Tack Saquai,^{1,†} Kenta Hongo,² Ryo Maezono,³ and Tom Ichibha^{1,‡}

¹*School of Information Science, JAIST, Asahidai 1-1, Nomi, Ishikawa 923-1292, Japan*

²*Center for Advanced Scientific Computing, JAIST, Asahidai 1-1, Nomi, Ishikawa 923-1292, Japan*

³*Graduate Major in Materials and Information Sciences, School of Materials and Chemical Technology, Institute of Science Tokyo 2-12-1-S6-22 Ookayama, Meguro-ku, Tokyo 152-8550, Japan.*

(Dated: May 26, 2026)

In first-principles design of solid solutions and disordered materials, evaluating the energies of all possible configurations is generally impractical because the number of substitutional-site occupations increases exponentially. In this study, we developed a framework that applies annealing methods to the pre-screening of mixed-crystal configurations using electrostatic energy, specifically Ewald energy, as the objective function, and systematically evaluated its effectiveness. The occupation states of substitutional sites were represented by binary 0/1 variables, and the Ewald energy was mapped onto an Ising-type Hamiltonian. This formulation allowed the search for low-electrostatic-energy configurations to be treated as a combinatorial optimization problem. The formulation was implemented using simulated annealing (SA) and quantum annealing (QA), and their performance was quantitatively assessed by comparison with exhaustive search in terms of speed-up factors and the ability to identify the lowest-energy structures. For the small-scale system CaYAlO_4 , SA achieved a speed-up of approximately 30 times, while QA achieved a speed-up of more than 100 times; both methods successfully captured the lowest-energy configurations without missing any of them. For the medium-scale system $\beta\text{-KSbF}_4$ and the large-scale Ba-doped SiAlON system, SA achieved speed-ups on the order of 200–300 times while stably identifying the lowest-energy structures. In contrast, although QA was effective for the small-scale system, its speed-up was limited for medium-scale problems, and some low-energy configurations were missed due to chain breaks. These results demonstrate that, for mixed-crystal configuration search based on electrostatic energy, SA is currently the most robust and general-purpose method for rapid pre-screening and is practically applicable even to large-scale problems. The formulation presented in this study can be implemented automatically using publicly available libraries and, when integrated stepwise with first-principles calculations, provides a computational framework that can accelerate candidate-structure generation and property prediction for real materials systems.

I. INTRODUCTION

In the materials design of solid solutions and disordered systems, properties are often tuned to a desired range by introducing dopants such as cations, anions, or vacancies [1]. When such systems are treated using first-principles calculations, one must confront the combinatorial number of possible elemental arrangements at the substitutional sites [2, 3]. This number can increase exponentially with the number of substitutional sites [3]. For example, in the structural model of $\text{Zn}_{0.5}\text{Fe}_2\text{Cu}_{0.5}\text{O}_4$ reported in COD 9012442 [4], as many as 127,400 symmetry-distinct configurations are possible within the unit cell specified therein. In magnetic systems, the number can become even larger because substitutional sites occupied by the same ionic species may still be classified as inequivalent depending on their spin orientations, reaching as many as 1,229,107,765,600 possible configurations [5].

These configurations generally have different energy values[6]. However, in practical first-principles simulations, the configurations that should be considered are usually limited to a subset of patterns with sufficiently low and physically realizable energies[7]. The most straightforward proce-

cedure for identifying such configurations would be to perform structural relaxation using first-principles calculations for all possible substitutional-site occupation patterns, compare their energies, identify the most stable structures, and then proceed to property calculations. However, screening hundreds of millions or even trillions of structures by evaluating their energies one by one using first-principles calculations is not practically feasible.

This naturally leads to a strategy in which configurations are screened not by using accurate energy values, but by using an alternative descriptor that can be evaluated much more rapidly. One possible descriptor for this purpose is the electrostatic energy [8]. The total energy of a material system is determined by the distribution of many interacting electrons on top of the classical electrostatic interaction energy arising from the ionic arrangement [9]. First-principles calculations are designed to treat the delicate balance associated with the former electronic contribution [9, 10]. In ionic crystals, however, the relative stability of possible substitutional-site configurations can often be governed primarily by the latter electrostatic interaction [8, 11]. This electrostatic contribution is commonly discussed in terms of the Ewald energy. The Ewald energy can be evaluated much faster than a first-principles calculation. For example, in the present system, its evaluation is approximately 43,000 times faster. Extrapolating this speed-up to all 127,400 configurations, the screening would require approximately 146,000 h using first-principles calculations,

*

[†] mwkskt2308@gmail.com

[‡] ichibha@gmail.com

whereas it would take only about 3 h when based solely on Ewald-energy evaluations.

Software packages that can rapidly estimate Ewald energies are widely available [12, 13], and one might therefore expect that screening can simply be performed using such tools. However, even with this reduced evaluation cost, the computational time becomes prohibitive when realistic mixed-crystal materials are considered. For example, in the case of $(\text{Nd}_{0.7}\text{Ce}_{0.225}\text{La}_{0.075})_2\text{Fe}_{14}\text{B}$, even if the evaluation time is only about 0.1 s per configuration, the total number of possible configurations reaches 1,229,107,765,600, resulting in an unrealistic computational time of approximately 34,000,000 h, or about 3,880 years [5]. Thus, an exhaustive search over all possible substitutional-site occupation patterns is impractical. Since our ultimate interest lies in substitutional structures with low energies, it is desirable to develop a method that efficiently eliminates high-energy substitutional configurations and selectively extracts low-energy ones.

As a method for such selective extraction, we considered the application of annealing methods [14]. To implement an annealing method, it is necessary to formulate a model in which the objective function is expressed in terms of binary variables. This enables the optimization problem to be mapped onto the problem of searching for the most stable spin configuration. As described in §II, the occupation of substitutional sites can be represented by 0/1 binary variables, and the Ewald energy can be expressed as a function of these binary variables, which we refer to as the annealing model. By using this value as the objective function, the problem can be formulated as a combinatorial optimization problem in which one searches for a bit string that gives a lower Ewald energy. In general, combinatorial optimization problems are algorithmically challenging because they are often accompanied by multimodality [15]. Heuristic search methods for addressing such problems have therefore been actively studied. Examples include genetic algorithms [16, 17], particle swarm optimization [18, 19], and Bayesian optimization [20, 21]. For an objective function expressed in terms of binary variables, annealing techniques can be applied by mapping the problem onto a spin Hamiltonian. More specifically, the problem can be recast as the search for the spin configuration that realizes the lowest energy. This problem can be solved using methods such as quantum annealing [5, 7] and simulated annealing [15].

As described in §III, annealing-based extraction of low-energy substitutional structures does not necessarily guarantee complete coverage of all low-energy candidates. Although a previous study demonstrated that quantum annealing can mitigate this issue [14], the extent of the speed-up achievable by annealing methods and their ability to recover all relevant low-energy structures without omission have not been quantitatively clarified. The present study therefore aims to evaluate these two aspects systematically.

Based on the above considerations, the objective of the present study is defined as follows. We consider Ewald-energy-based screening of a large number of substitutional

structural models for mixed-crystal systems of inorganic compounds. The Ewald energy is expressed as an annealing model, and the problem is formulated as a combinatorial optimization problem in which the binary variables that minimize the energy are searched for. This combinatorial optimization problem is implemented using simulated annealing [15] and quantum annealing [22]. By comparing the results with those obtained by exhaustive search, we quantitatively evaluate the speed-up achieved by annealing methods and their ability to identify low-energy structures without omission.

In this study, we selected three compounds according to the number of possible substitutional-site configurations, which corresponds to the difficulty of the combinatorial optimization problem: CaYAlO_4 , which has a relatively small number of configurations; $\beta\text{-KSbF}_4$, which has a more realistic problem size; and Ba-doped SiAlON , which represents an even larger-scale system. In selecting these compounds, we chose systems in which the ions substituted in the mixed crystal have valences different from those of the host ions, so that the Ewald energy, used as the objective function, varies among different configurations.

For the small-scale system CaYAlO_4 , both simulated annealing and quantum annealing were able to efficiently extract only mixed-crystal configurations with low Ewald energies. Compared with the conventional exhaustive search, simulated annealing achieved a speed-up of nearly 30 times and identified the lowest-energy structures without missing any candidates. For a problem of this size, quantum annealing performed even faster, achieving a speed-up of more than 100 times while also identifying the lowest-energy structures without omission. For $\beta\text{-KSbF}_4$, which represents a realistic level of difficulty, simulated annealing achieved a speed-up of more than 200 times depending on the cooling schedule. In contrast, quantum annealing did not exhibit sufficient performance. This was attributed mainly to constraints in the implementation of physical qubits, such as chain breaks. This finding provides new insight that was not discussed in the previous study [14]. Simulated annealing also achieved a speed-up of more than 300 times for Ba-doped SiAlON , an even larger and more challenging system. These results indicate that mixed-crystal configuration search can potentially be performed extremely rapidly when formulated as an annealing problem. At the same time, they also show that, for quantum annealing to fully demonstrate its performance in this direction, constraints arising from the current implementation of physical qubits remain an important issue.

The remainder of this paper is organized as follows. In §II, we describe the formulation and implementation of the Ewald-energy evaluation of substitutional-site configurations as a combinatorial optimization problem by mapping it onto an Ising-type Hamiltonian and applying annealing methods. We also describe the target systems used for validation. In §III, we evaluate the performance of simulated annealing and quantum annealing for systems of different sizes by comparing their search results with those obtained by exhaustive search. We also discuss, from the viewpoint of chain breaks, the factors that cause quantum annealing to miss optimal solu-

tions in medium-scale and larger systems. Finally, §IV summarizes the conclusions of this study.

II. METHOD

We consider the Ewald energy E of a periodic system with site substitutions in a solid solution. Let q_i denote the charge of a site that can be substituted, and Q_k denote the charge of a site that is known in advance not to be substituted, where i and k are site indices. The Ewald energy E can be expressed as a superposition of pairwise interactions:

$$E = \sum_j \sum_{i \leq j} A_{ij} q_i q_j + \sum_k \sum_{l \leq k} B_{kl} Q_k Q_l + \sum_k \sum_i C_{ki} Q_k q_i \quad (1)$$

where A_{ij} , B_{kl} , and C_{ki} are interaction coefficients determined solely by the geometric arrangement of the sites.

Whether the site charge q_i is actually substituted or not can be represented by a binary variable $\sigma_i = 0$ or 1 . Let $q_i^{(0)}$, and $q_i^{(1)}$ denote the charges before and after substitution, respectively. Then, q_i can be written as

$$q_i = (1 - \sigma_i) \cdot q_i^{(0)} + \sigma_i \cdot q_i^{(1)} \quad (\sigma_i = 0 \text{ or } 1) \quad (2)$$

Substituting Eq. (2) into Eq. (1), the energy can be rearranged into the form of an Ising-type Hamiltonian as

$$E \sim \sum_{i \leq j} J_{ij} \sigma_i \sigma_j + \sum_i h_i \sigma_i + \text{const.} \quad (3)$$

The original electrostatic interaction coefficients A_{ij} , B_{ij} , and C_{ij} can be determined once the crystal structure is specified. Therefore, the model parameters J_{ij} and h_i can be obtained from these coefficients.

Thus, each possible substitutional-site occupation state can be represented as spin configuration $\sigma = (\sigma_1, \sigma_2, \dots, \sigma_N)$. The problem can therefore be recast as an annealing problem in which the Ising-type Hamiltonian is minimized over all possible spin configurations $\{0, 1\}^N$.

To restrict the search space to solid solutions with a prescribed site substitution ratio, an additional constraint term is added to Eq. (3). Let α be an index that distinguishes the types of substitutional sites, such as elemental species or inequivalent Wyckoff positions, and let N_α denote the total number of substituted sites corresponding to each substitution ratio. The Hamiltonian is then given by

$$H_{\text{ewald}} = \sum_{i \leq j} J_{ij} \sigma_i \sigma_j + \sum_i h_i \sigma_i + \lambda \sum_\alpha \left(\sum_{i \in \alpha} \sigma_i - N_\alpha \right)^2. \quad (4)$$

Here, λ is a coefficient that controls the strength of the constraint. Specifying the substitutional composition of a solid solution corresponds to specifying the set (N_1, N_2, \dots) . Using H_{ewald} as the objective function, we performed a search for the optimal Ising spin configuration $\sigma = (\sigma_1, \sigma_2, \dots, \sigma_N)$

that minimizes this function, using simulated annealing and quantum annealing.

As target systems, we considered several compounds according to the number of possible substitutional-site configurations, which corresponds to the difficulty of the combinatorial optimization problem. We selected CaYAlO₄ [23] as the small system with the smallest number of configurations, and β -KSbF₄ [24] as the medium system with a more realistic problem size. For simulated annealing, we also considered Ba-doped SiAlON [25] as a large and more challenging system with an even larger number of configurations. The calculations were performed using a $1 \times 2 \times 2$ supercell for CaYAlO₄, a $1 \times 1 \times 2$ supercell for β -KSbF₄, and a $2 \times 2 \times 1$ supercell for Ba-doped SiAlON. With this choice of supercells, all elements of the set $\{N_\alpha\}$ can be taken as integers. A comparison of the number of possible substitutional configurations for these systems is shown in Table I. In these compounds, the substituting ions have valences different from those of the ions being substituted. Therefore, the Ewald energy, which serves as the objective function for optimization, varies among different configurations, making these systems suitable test cases for optimization. CaYAlO₄ is an important host material for phosphors and lasers [26, 27], β -KSbF₄ is an important ionic conductor [24, 28], and Ba-doped SiAlON is an important host material for phosphors [29].

To implement annealing based on Eq. (4), we used two methods in this study: simulated annealing (SA) and quantum annealing (QA). In both methods, we perform M independent annealing runs and obtain one spin configuration as a sample from each run. These samples are then individually annealed toward solutions of Eq. (4), and the resulting spin configurations are observed. The way in which this relaxation process is implemented differs between SA and QA. The observed set of M Ising spin configurations, $\{\sigma^{(j)}\}_{j=1}^M$, corresponds to M substitutional-site configurations that realize low-energy states. In this way, substitutional-site configurations can be obtained.

For simulated annealing, we used the `dwave-samplers` library. The number of samples M was set to 30 for CaYAlO₄, 250 for β -KSbF₄, and 5,000 for Ba-doped SiAlON (Table I). In simulated annealing, the temperature associated with the Boltzmann factor for Eq. (4) is gradually decreased from a high temperature to a low temperature. At each temperature step, the spin configuration is relaxed toward equilibrium according to the Boltzmann factor at that temperature. This procedure is repeated while updating the temperature step by step. The rule used to update the temperature is called the cooling schedule. For the cooling schedule in this study, we applied and compared geometric cooling,

$$\beta_{k+1} = \left(\frac{\beta_N}{\beta_1} \right)^{\frac{1}{N-1}} \beta_k, \quad (1 \leq k \leq N-1) \quad (5)$$

and linear cooling,

$$\beta_{k+1} = \beta_k + \frac{\beta_N - \beta_1}{N-1}, \quad (1 \leq k \leq N-1) \quad (6)$$

TABLE I. Number of substitutional sites in the simulation cell and the number of possible substitutional configurations. ‘SA[G]’ and ‘SA[L]’ denote simulated annealing with geometric and linear cooling schedules, respectively, and ‘QA’ denotes quantum annealing. The values listed for these methods indicate the speed-up factors relative to exhaustive search. Because the speed-up depends on the computational conditions of the annealing methods, the listed values should be interpreted as representative speed-up factors achieved in the present calculations. For the largest system, Ba-doped SiAlON, the QA result is not shown because the calculation could not be performed, and the SA[L] result is omitted because low-energy configurations were missed.

Target system	Number of mixed-crystal sites	Number of possible substitutional configurations	Number of symmetrically inequivalent structures	Number of samples	SA[G]	SA[L]	QA
CaYAlO ₄ (1 × 2 × 2)	8	70	10	30	26.6	43.8	116
β-KSbF ₄ (1 × 1 × 2)	18	794	52	250	18.8	248	1.29
Ba-doped SiAlON (2 × 2 × 1)	24	127,400	31,976	5,000	286	–	–

TABLE II. Computational environment used for exhaustive search and simulated annealing

Item	Specification
CPU	Apple M3
Number of CPU cores	8
Memory	16 GB

where β_k is the inverse temperature at the k -th step. These equations represent the cooling update schemes over N steps. In the `dwave-samplers` library, the initial value β_1 and the final value β_N used for the update are given by

$$\beta_1 = \frac{\log_e 2}{\Delta E_{\max}}, \quad \beta_N = \frac{\log_e 100}{\Delta E_{\min}}.$$

Here, ΔE_{\max} and ΔE_{\min} are, respectively, the approximate upper and lower bounds on the absolute value of the energy change ΔE that occurs when a single spin is flipped from an arbitrary spin configuration σ . This means that, at the initial stage, even the largest energy increase is accepted with a probability of 50%, thereby enabling global exploration. At the final stage, even the smallest energy increase is accepted with a probability of only 1%, thereby promoting convergence to an optimal solution. The total number of steps used for cooling, N , is referred to as the number of sweeps. In this study, we basically adopted geometric cooling with $N = 1,000$ sweeps. This value is the default setting in the `dwave-samplers` library.

For the hardware implementation of quantum annealing, we used D-Wave’s Advantage system 4.1 QPU [30]. The Hamiltonian was embedded onto the quantum computer using the `AutoEmbeddingComposite` in the Ocean SDK [31]. In quantum annealing, the search for the optimal solution is performed by taking an equal superposition of all possible states, namely the Hadamard state, as the initial state and evolving the system toward the ground state of the given Hamiltonian [22]. This operation is realized by varying the Hamiltonian with time. Specifically, the time-dependent Hamiltonian is taken as the linear combination of the transverse-field term H_{trans} , whose ground state is the Hadamard state, and the problem Hamiltonian H_{ewald} :

$$H(t) = A \left(\frac{t}{\tau} \right) \cdot H_{\text{trans}} + B \left(\frac{t}{\tau} \right) \cdot H_{\text{ewald}}, \quad (0 \leq t \leq \tau). \quad (7)$$

The Hamiltonian is then varied with time t . The functions $A(s)$ and $B(s)$ are determined by the implementation of the quantum computer. They satisfy $A(s) \gg B(s)$ at $s = 0$ and $A(s) \ll B(s)$ at $s = 1$. In other words, as s increases, the contribution of the transverse-field term approaches zero. Here, τ is called the annealing time and determines the rate at which the contribution of the transverse-field term is reduced. In this study, τ was varied in the range from 20 μs to 2,000 μs . According to Eq. (7), the effective coupling constants between Ising spins are varied over the time interval $t = [0, \tau]$, and the relaxed spin configurations are obtained. The number of samples M was set to 30 for CaYAlO₄ and 250 for β -KSbF₄.

In quantum annealing, the ideal implementation is that each Ising variable is represented by a single qubit. However, owing to technical constraints, a workaround is used in which a single Ising variable is represented by multiple physical qubits [32]. A group of physical qubits corresponding to a single Ising variable is called a chain. Ideally, all physical qubits forming a chain are expected to take the same state. In practice, however, an undesired situation often occurs in which the physical qubits within a chain do not take the same state. This situation is referred to as a chain break. Chain breaks will be discussed later in this paper. When a chain break occurs, we determine the corresponding Ising variable by taking a majority vote over the states of the physical qubits in the chain. The physical qubits within a chain are coupled ferromagnetically so that they tend to take the same state. The strength of this coupling is a hyperparameter called the chain strength, denoted by μ . Increasing the chain strength makes chain breaks less likely to occur. On the other hand, it is known that an excessively large chain strength can degrade the performance in finding the optimal solution [33]. Therefore, the chain strength should not simply be made as large as possible; an appropriate value must be selected.

In addition to the chain strength, another tunable hyperparameter is the coefficient λ of the constraint term in Eq. (4). Although these hyperparameters should be appropriately determined depending on the problem, no general method for determining their optimal values has been established, and this remains an active area of research [34–36]. The value of λ was determined by monitoring whether the constraint represented by the corresponding constraint term was satisfied. When λ is sufficiently large, the constraint is satisfied. We then gradually reduced this value and identified the smallest value for which

the constraint was satisfied as well as possible. For simulated annealing, we used $\lambda^{(\text{SA})} = 50$ eV for all systems. For quantum annealing, we used $\lambda^{(\text{QA})} = 150$ eV for the small-scale system CaYAlO_4 and $\lambda^{(\text{QA})} = 700$ eV for the medium-scale system $\beta\text{-KSbF}_4$. The chain strength μ was determined by searching for a value that made the chain-break fraction B as small as possible. We used $\mu = 250$ for the small-scale system CaYAlO_4 and $\mu = 1,400$ for the medium-scale system $\beta\text{-KSbF}_4$.

For calibration of the results, we also reconstructed the set of charges $\{q_i\}$ from each spin configuration $\sigma = (\sigma_1, \sigma_2, \dots, \sigma_N)$ and evaluated the Ewald energy using Eq. (1). This enables a direct comparison with the Ewald-energy evaluation performed by the conventional exhaustive search, in terms of both the calculated energy values and the computational cost. For the calculated energy values, the difference between the two approaches was confirmed to be on the order of 10^{-9} eV or less per simulation cell.

Simulated annealing and exhaustive search were performed on the computer with the specifications listed in Table II. In the exhaustive search, the Ewald energy was evaluated sequentially for all substitutional configurations, including symmetrically equivalent ones.

III. RESULTS AND DISCUSSION

For both the small- and medium-scale systems, simulated annealing showed good performance improvement for all systems. In contrast, quantum annealing achieved sufficient performance improvement only for the small-scale system, owing to limitations in the current hardware implementation, and its performance improvement was limited for the medium-scale system (Table I). In this section, we first present the results of simulated annealing (§III A), followed by the results obtained when the same problem was applied to quantum annealing (§III B). Optimization is expected to proceed more easily when the number of binary variables describing the system is smaller, that is, when the number of substitutional sites in the crystal is smaller. Therefore, we begin with the small-scale system, then increase the system size, and compare the results. We then examine the case of a larger-scale system (§III C) and the effect of the cooling schedule in SA (§III D). Finally, we discuss the factors responsible for the omission of optimal solutions in QA (§III E).

A. Simulated annealing for small- and medium-scale systems

Figure 1 shows the results obtained by applying simulated annealing to the small-scale system [panel (a)] and the medium-scale system [panel (b)]. Here, the default geometric cooling schedule was used. The results obtained with linear cooling are described later in §III D. In this figure, the horizontal axis represents the energy values of the sampled site-substitution patterns, and the vertical axis shows the number of configurations in each energy range as a histogram. Be-

cause the number of possible atomic configurations is limited, the histogram appears discretely. In constructing the histogram, we also took into account the fact that configurations that are different as spin configurations can be identical as crystal structures owing to spatial symmetry. Therefore, the vertical axis represents the accumulated number of mutually inequivalent crystal structures belonging to the same energy range. If the histogram obtained by exhaustive search (black) is not fully covered by that obtained by the annealing method (red), this indicates that some crystal structures were missed by the annealing method. Since the purpose of pre-screening is to extract the crystal structures with the lowest energy, the key point is whether the red histogram fully covers the lowest-energy bin.

For both the small-scale system [panel (a)] and the medium-scale system [panel (b)], the distributions shown in red indicate that simulated annealing did not sample high-energy crystal structures, but selectively sampled energetically stable structures. With no more than $M = 30$ samples for the small-scale system and $M = 250$ samples for the medium-scale system, all crystal structures belonging to the lowest-energy level were captured. For the medium-scale system, the time required to obtain $M = 250$ samples was 0.0344(3) s. In contrast, 0.646 s was required to compare the Ewald energies by exhaustive search, corresponding to the black histogram in the figure. Therefore, simulated annealing enabled the stable structures to be searched approximately 18.8 times faster.

B. Quantum annealing for small- and medium-scale systems

Having shown that annealing methods are effective for improving the efficiency of the search, it is natural to examine whether quantum annealing can achieve a more substantial speed-up. Annealing methods are designed to enable global search by escaping from local minima through mechanisms that overcome energy barriers [15, 22]. In simulated annealing, transitions to higher-energy states are accepted according to probabilities determined by the Boltzmann distribution, allowing the system to overcome energy barriers within a classical algorithmic framework [15]. In contrast, quantum annealing utilizes quantum superposition to explore many candidate states and uses quantum tunneling to pass through energy barriers, thereby driving the system toward the global optimum [22]. Because this procedure is expected to exploit quantum-mechanical parallelism, it has been regarded as a method that can potentially achieve a substantial speed-up over classical implementations [37]. However, in practical quantum annealing hardware, there are technical limitations on both the number of physical qubits and the number of couplings among them. Therefore, as the system size increases, the speed-up achievable with current hardware is expected to become limited [37].

First, the results for the small-scale system CaYAlO_4 are shown in Fig. 2. As in the case of simulated annealing, the high-energy structure (-212 eV/f.u.) was not sampled, indicating that stable structures were selectively sampled. Since

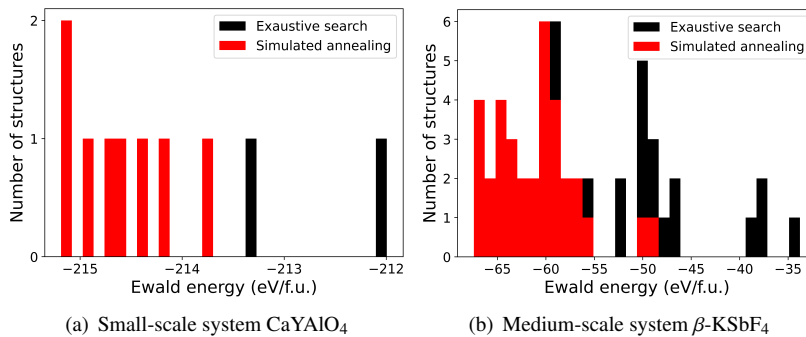


FIG. 1. Distributions of Ewald energies for all symmetrically inequivalent mixed-crystal structures obtained by exhaustive search (black) and for the structures obtained by simulated annealing (red) in (a) the small-scale system CaYAIO₄ and (b) the medium-scale system β -KSbF₄. The Ewald energy is given in eV per formula unit. The red distributions cover the low-energy regions, indicating that low-energy substitutional-site configurations were captured without omission.

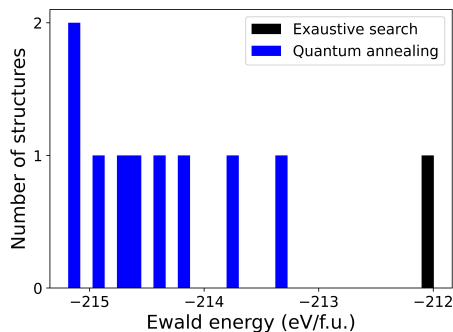


FIG. 2. Distribution of Ewald energies for symmetrically inequivalent structures in the small-scale system CaYAIO₄ obtained by exhaustive search (black) and for the structures obtained by quantum annealing (blue). The Ewald energy is given in eV per formula unit.

the search was performed with an annealing time of 20 μ s per sample, obtaining $M = 30$ samples required 600 μ s. The exhaustive search for this system was estimated to require 70,000 μ s; thus, quantum annealing achieved a speed-up of 116 times compared with exhaustive search.

Next, the results obtained by applying quantum annealing to the medium-scale system β -KSbF₄ are shown in Fig. 3. Results are shown for three annealing times: $\tau = 20$ μ s [panel (a)], $\tau = 200$ μ s [panel (b)], and $\tau = 2,000$ μ s [panel (c)]. For $\tau = 20$ μ s [panel (a)], which showed sufficient search performance for the small-scale system [Fig. 2], the crystal structures belonging to the lowest-energy range were not fully captured; the blue histogram obtained by quantum annealing does not fully cover the black histogram obtained by exhaustive search. As τ was increased and the search time was extended, the low-energy structures were captured more completely. At $\tau = 2,000$ μ s [panel (c)], all crystal structures in the lowest-energy range were captured. In this case, the calculation required 0.5 s. Since exhaustive search is known to require 0.646 s, the speed-up achieved by quantum annealing under this condition is reduced to a factor of 1.29.

C. Simulated annealing results and computational cost for the large-scale system

In terms of omission, the performance of quantum annealing was limited at the size of the medium-scale system β -KSbF₄, whereas simulated annealing showed good performance. We therefore examined whether this performance could be maintained for a larger system. As the target system, we selected the large-scale Ba-doped SiAlON system with a $2 \times 2 \times 1$ supercell. This system contains 24 substitutional sites, yielding 127,400 possible substitutional configurations and 31,976 symmetrically inequivalent structures. The number of samples was set to $M = 5,000$. The results are shown in Fig. 4.

Because this system has a large total number of configurations, the histogram bins are distributed almost continuously. In simulated annealing, taking 5,000 samples was sufficient to capture all lowest-energy substitutional structures without omission. This sampling was completed in 1.010(6) s. In contrast, exhaustive search required 289.07 s in total. Thus, simulated annealing achieved sampling that was 286 times faster.

The main focus of this paper is the speed-up achieved by annealing methods. As shown in the results, speed-ups of more than two orders of magnitude can be achieved when the performance is evaluated solely in terms of computational time. Nevertheless, there is an additional human cost associated with reformulating the original problem as a Hamiltonian suitable for annealing. As discussed in the Introduction, if the conventional exhaustive search is itself infeasible, this human cost does not constitute a serious drawback, because there is no practical alternative for overcoming the combinatorial explosion. Even so, it is meaningful to clarify the human cost required to construct the Hamiltonian for annealing.

When the CIF file of the parent crystal, the substituting ions, and the substitution ratios are provided as input to the Pymatgen library [12], the Ewald-energy term in Eq. (1) can be constructed. In the case of Ba-doped SiAlON, for which the number of possible substitutional configurations reaches 127,400, this construction requires only 0.78 s. The con-

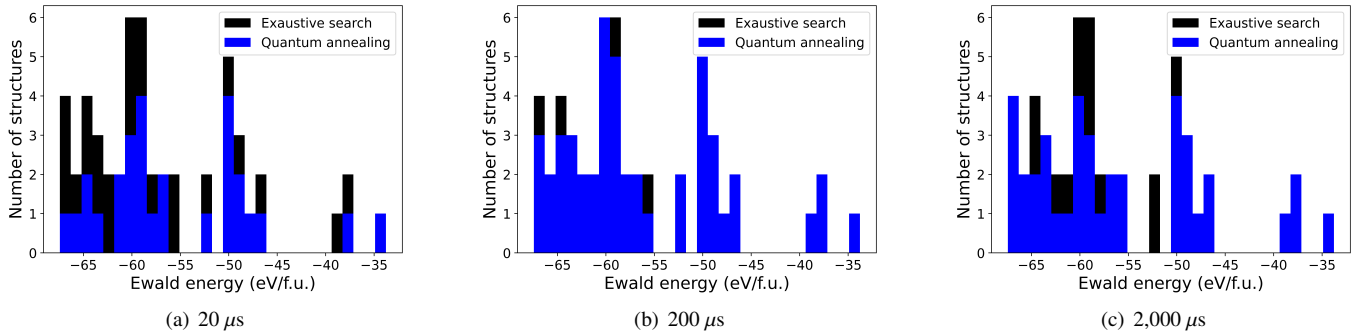


FIG. 3. Distribution of Ewald energies for symmetrically inequivalent structures in the medium-scale system β -KSbF₄ obtained by exhaustive search (black), and distributions of structures obtained by quantum annealing (blue) with annealing times of (a) 20 μ s, (b) 200 μ s, and (c) 2,000 μ s. The number of samples was fixed at 250, and the Ewald energy is given in eV per formula unit.

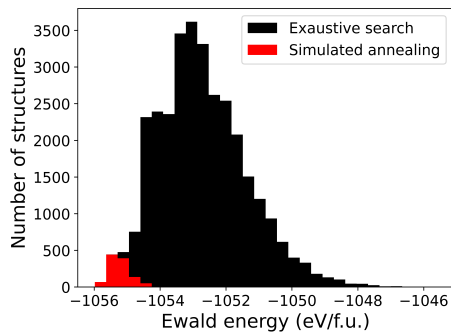


FIG. 4. Distribution of Ewald energies for all symmetrically inequivalent mixed-crystal structures in the large-scale Ba-doped SiAlON system obtained by exhaustive search (black), and the distribution of structures obtained by simulated annealing (red). The Ewald energy is given in eV per formula unit. The red distribution fully covers the low-energy region, indicating that low-energy substitutional-site configurations were captured without omission.

straint term can also be constructed from the same information using the library; this step requires 0.000097 s. By passing the calculated objective and constraint terms to the Python library pyqubo [38], the Ising Hamiltonian including the constraint term can be constructed; this step requires 0.00087 s. Simulated annealing is then performed for the resulting Ising Hamiltonian using the dwave-samplers library. All Python libraries used in this procedure are publicly available. Thus, the overall workflow can be executed mechanically using automated libraries and does not require substantial human effort.

D. Comparison between geometric and linear cooling in SA

The simulated annealing calculations presented so far were performed using the default geometric cooling schedule. When this schedule was replaced by linear cooling, an improvement in computational speed was observed. However, for the large-scale system, it was also found that some low-energy structures were missed.

Figure 5(a) shows the results obtained by applying simulated annealing with linear cooling to the small-scale system CaYAIO₄. The histogram indicates that the sampling was concentrated in the low-energy region also for this system. In this case, no more than $M = 30$ samples were taken, and all structures belonging to the lowest-energy bin were obtained. This sampling was completed in 0.00160(2) s, corresponding to a speed-up factor of 43.8 relative to the 0.070 s required for exhaustive search.

Figure 5(b) shows the results obtained by applying simulated annealing with linear cooling to the medium-scale system β -KSbF₄. The histogram indicates that the sampling was concentrated in the low-energy region also for this system. In this case, no more than $M = 250$ samples were required to obtain all structures belonging to the lowest-energy bin. This sampling was completed in 0.00260(3) s, corresponding to a speed-up factor of 248 relative to the 0.646 s required for exhaustive search.

Figure 5(c) shows the results obtained by applying simulated annealing with linear cooling to the large-scale Ba-doped SiAlON system. The histogram indicates that the sampling was concentrated in the low-energy region also for this system. In this case, using $M = 5,000$ samples was not sufficient to obtain all structures belonging to the lowest-energy bin, and some structures were confirmed to be missed. This sampling was completed in 0.051(3) s, which is 5,658 times faster than the 289.07 s required for exhaustive search. However, because some structures were missed, this achieved performance is not listed in Table I.

As described above, linear cooling, similarly to geometric cooling, sampled structures preferentially in the low-energy region. Except for the large-scale system, it was able to obtain all structures belonging to the lowest-energy bin without omission. It was also shown that linear cooling can be evaluated faster than geometric cooling.

The main causes are considered to be the increased number of accepted spin changes that raise the energy and the associated increase in the time required to evaluate energy changes. In simulated annealing, spin changes that increase the energy

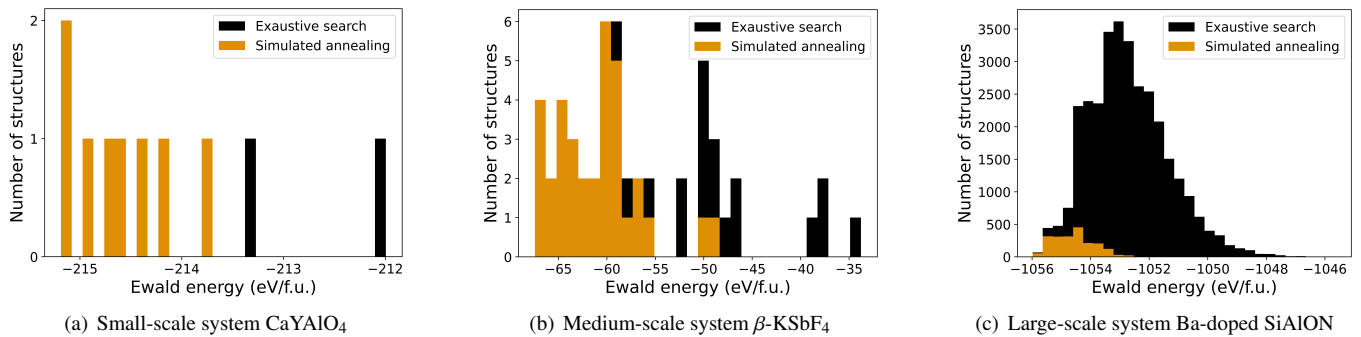


FIG. 5. Distribution of Ewald energies for symmetrically inequivalent structures obtained by exhaustive search (black), and distributions of structures obtained by simulated annealing with linear cooling (orange) for (a) the small-scale system CaYAlO_4 , (b) the medium-scale system $\beta\text{-KSbF}_4$, and (c) the large-scale Ba-doped SiAlON system. The Ewald energy is given in eV per formula unit.

are also accepted with a probability determined by the Boltzmann distribution. For each spin change, it is therefore necessary to first evaluate how much the energy would increase and then calculate the corresponding Boltzmann factor. In the *dwave-samplers* library, the energy change associated with flipping each spin is stored in advance and used for the acceptance test. Because this energy change depends on the spin configuration, when a spin flip is accepted and the configuration changes, the stored energy changes for the other affected spins must also be updated. In other words, the energy changes are not recalculated from scratch at every step; instead, the values for the relevant spins are sequentially updated according to the accepted spin flips. Therefore, as the number of accepted spin flips increases, the number of such update operations also increases, resulting in an increase in the time required to update the energy changes.

Compared with linear cooling, geometric cooling resulted in a larger number of accepted spin flips that increased the energy, by factors of 2.60 for the small-scale system CaYAlO_4 , 117.7 for the medium-scale system $\beta\text{-KSbF}_4$, and 183.8 for the large-scale Ba-doped SiAlON system, on average. Correspondingly, the time required to update the energy changes was also longer for geometric cooling, by factors of 2.59 for CaYAlO_4 , 117.2 for $\beta\text{-KSbF}_4$, and 187.6 for Ba-doped SiAlON, on average.

The reason why energy-increasing changes occurred more frequently with geometric cooling than with linear cooling can be understood as follows. In the *dwave-samplers* library, the inverse temperature is updated according to Eqs. (5) and (6). The inverse temperature gradually increases with the temperature step. In linear cooling, the increment of the inverse temperature is constant with respect to the temperature step. In contrast, in geometric cooling, the increment is small in the early stage and becomes large in the final stage. In other words, geometric cooling keeps the system in the low-inverse-temperature region for a longer period. In this region, the Boltzmann factor corresponding to the inverse temperature becomes larger, and energy-increasing spin flips are therefore more likely to be accepted. Thus, because geometric cooling remains longer in the low-inverse-temperature region than

linear cooling, a larger number of energy-increasing spin flips are considered to have been accepted. As a result, the time required to update the energy changes also increased, leading to a longer computational time than that for linear cooling.

In addition, we confirmed that the omission observed for the large-scale Ba-doped SiAlON system can be improved by the following two approaches. The first approach is to increase the number of sweeps by a factor of four to $N = 20,000$. This corresponds to slower cooling. Under this condition, $M = 5,000$ samples were obtained for the large-scale system in 0.90(7) s, corresponding to a speed-up factor of 321 relative to exhaustive search, and no omission was observed. Considering that geometric cooling achieved a speed-up factor of 286, increasing the number of sweeps in linear cooling can be regarded as more effective for the large-scale Ba-doped SiAlON system. On the other hand, when the same condition was applied to the other systems, the speed-up factors relative to exhaustive search were 2.26 for the small-scale system CaYAlO_4 and 13.4 for the medium-scale system $\beta\text{-KSbF}_4$. Although no omission was observed in either case, the corresponding speed-up factors obtained with geometric cooling were 26.6 and 18.8, respectively. Therefore, under this condition, linear cooling is slower than geometric cooling for these systems.

The second approach is to increase the number of samples. When the number of samples was increased to $M = 40,000$, no omission was observed, and the search was completed in 0.433(5) s. This corresponds to a speed-up factor of 668 relative to exhaustive search, which is faster than the speed-up factor of 286 obtained with geometric cooling. For the large-scale Ba-doped SiAlON system, omission was eliminated by using eight times more samples than in the case of geometric cooling. Therefore, we also performed sampling for the small- and medium-scale systems using the same eightfold increase in the number of samples. As expected, no omission was observed, as in the original sampling. The speed-up factors relative to exhaustive search were 5.69 for the small-scale system CaYAlO_4 and 30.2 for the medium-scale system $\beta\text{-KSbF}_4$. Under this condition, linear cooling was faster than geometric cooling for the medium-scale and larger systems,

whereas it was slower for the small-scale system.

As described above, whether linear cooling or geometric cooling is faster depends on the size of the target system. Therefore, the superiority of one over the other cannot be determined uniquely on the basis of computational time alone. It is then meaningful to compare the two cooling schedules from the viewpoint of search performance, namely the probability of obtaining all structures belonging to the most stable energy bin without omission when the annealing method is applied multiple times. Here, multiple trials do not mean the M combinatorial optimizations corresponding to the number of samples. Rather, they mean repeating the entire set of M combinatorial optimizations multiple times. In other words, for each annealing condition described above, we evaluated the probability with which all structures belonging to the most stable energy bin can be obtained without omission.

These results are summarized in Table IV. For comparison, the results for simulated annealing with geometric cooling and quantum annealing are also included.

For simulated annealing, linear cooling with an increased number of sweeps outperformed geometric cooling only for the small-scale system CaYAlO_4 , whereas it performed worse than geometric cooling for the other systems. Linear cooling with an increased number of samples obtained the lowest-energy bin without omission for the small-scale system CaYAlO_4 and the medium-scale system $\beta\text{-KSbF}_4$. However, for the large-scale Ba-doped SiAlON system, the probability of obtaining the lowest-energy bin without omission was lower than under the other conditions, indicating that omissions were more likely to occur.

Thus, for simulated annealing, no single condition can be regarded as consistently superior to the others from both viewpoints: the speed-up factor and the probability of avoiding omissions.

On the other hand, the quantum annealing results in Table IV show lower values than those for simulated annealing for both the small-scale system CaYAlO_4 and the medium-scale system $\beta\text{-KSbF}_4$. Therefore, quantum annealing can also be regarded as inferior to simulated annealing in terms of the probability of avoiding omissions.

E. Omissions in quantum annealing

Revisiting Table I, quantum annealing, which was expected to show an advantage over simulated annealing, did not exhibit a speed-up for problems of realistic size. This is, of course, not necessarily an intrinsic limitation of quantum annealing itself, but is rather considered to arise from technical limitations in the current hardware implementation. In the present study, however, no problem such as failure of embedding due to an insufficient number of qubits occurred. Nevertheless, the quantum annealing calculations exhibited the problem of missing optimal solutions. This is one of the findings clarified in the present study.

There is a previous study that applied quantum annealing to electrostatic-energy evaluation using an approach similar to ours [14]. In the large-scale Ba-doped SiAlON system considered in the present study, the number of possible configurations is on the order of 10^5 . In contrast, that study treated LiCoO_2 , which has a much larger number of possible configurations, on the order of 10^{10} . They reported successful optimization by quantum annealing by adding a chemical-potential term, which modifies the curvature around the minimum of the objective function and thereby helps the calculation capture the optimal solution. Because their study targeted a system with a large number of configurations from the outset, they did not compare their results with exhaustive search over all configurations, as performed in the present study. Instead, they estimated the overall shape of the energy distribution over the target configuration space using the replica-exchange Monte Carlo method [39]. The replica-exchange Monte Carlo method samples various solutions according to Boltzmann distributions at different temperatures and exchanges samples obtained at different temperatures with a certain probability. This enables the search to escape from local optima and explore low-energy solutions. Therefore, rather than being equivalent to exhaustive search, this method is closer in spirit to the simulated annealing used in the present study, in the sense that it examines the distribution of accessible configurations by varying the temperature. Consequently, the previous study cannot be taken as conclusive evidence that low-energy substitutional configurations were exhaustively captured by quantum annealing. In the present study, we have clearly demonstrated that quantum annealing does not necessarily capture low-energy substitutional configurations efficiently and without omission.

It is then important to identify what constitutes the bottleneck that causes quantum annealing to fail to capture all low-energy substitutional configurations. It is also an important question whether such a problem can be overcome by future improvements in quantum annealing hardware implementations. A clear difference between the results for the small-scale system CaYAlO_4 and the medium-scale system $\beta\text{-KSbF}_4$ is the presence or absence of chain breaks. For the small-scale system CaYAlO_4 , no chain breaks occurred in any of the solutions. In contrast, for the medium-scale system $\beta\text{-KSbF}_4$, chain breaks occurred in some of the solutions. In this case, the chain-break fraction was distributed over the range from 5.55% to 33%. Benchmark studies have shown that when chain breaks occur, it becomes more difficult to reach low-energy solutions [40]. These observations suggest that chain breaks may be one of the factors that made the optimization of this system difficult.

We therefore examined whether chain breaks hinder the search for low-energy solutions in the medium-scale system $\beta\text{-KSbF}_4$ using an analysis method similar to that used in the previous study. The results are shown in Fig. 6. In this analysis, the chain-break fraction is plotted on the horizontal axis, and the average energy of the sampled solutions at each chain-break fraction is plotted on the vertical axis, allowing their correlation to be examined [40]. As in the previous study,

TABLE III. Results of simulated annealing with linear cooling. The values shown for these methods represent the speed-up factors achieved relative to exhaustive search. The speed-up naturally depends on the computational conditions used for the annealing method; therefore, the values reported here should be regarded as representative speed-up factors achieved in the present calculations. For comparison, the results of simulated annealing with geometric cooling (SA[G]) and quantum annealing (QA), listed in Table I, are also shown. In the results for linear cooling and quantum annealing shown here, no omission of the lowest-energy group of structures was observed.

System	Geometric cooling (SA[G])	Linear cooling with		Quantum annealing (QA)
		4 times more sweeps	8 times more samples	
CaYAlO ₄ (1 × 2 × 2)	26.6	2.26	5.69	116
β-KSbF ₄ (1 × 1 × 2)	18.8	13.4	30.2	1.29
Ba-doped SiAlON (2 × 2 × 1)	286	321	668	–

TABLE IV. Probability (%) of capturing the most stable energy bin without omission in simulated annealing and quantum annealing. The computational conditions for quantum annealing follow those under which no omission was confirmed in §III B.

System	Geometric cooling (SA[G])	Linear cooling with		Quantum annealing (QA)
		4 times more sweeps	8 times more samples	
CaYAlO ₄ (1 × 2 × 2)	71.1	72.5	100	50.5
β-KSbF ₄ (1 × 1 × 2)	99.2	98.5	100	64.7
Ba-doped SiAlON (2 × 2 × 1)	82.3	71.3	64.3	–

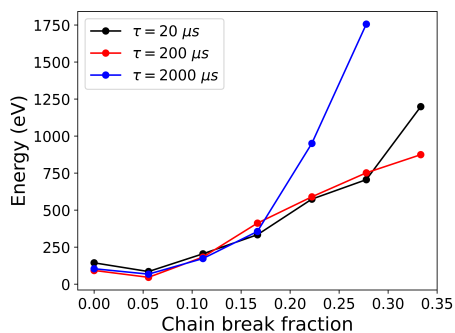


FIG. 6. Relationship between the chain-break fraction and solution quality for the medium-scale system β -KSbF₄. The horizontal axis represents the chain-break fraction in units of %, and the vertical axis represents the energy of the solutions in units of eV. Because solutions that do not satisfy the constraint term are also included, the energy is not given in eV per formula unit.

the results show an overall positive correlation. This supports the interpretation that, as chain breaks become more frequent, the search for low-energy solutions is hindered, resulting in a higher average energy of the sampled solutions. Although there are local regions where the average energy decreases, similar behavior was also observed in the previous study [40].

Low-energy substitutional structures extracted by quantum annealing were subject to omissions, and not all low-energy substitutional structures could be covered. Nevertheless, in practical applications, the demand is often not to ensure that the true optimal structure with an even lower energy than a given low-energy substitutional structure is captured, but rather to generate plausible low-energy substitutional structures, even partially, and proceed first to property evaluation. This pragmatic approach, in which promising candidate structures are selected as needed rather than exhaustively covering an enormous number of possibilities, is conceptually sim-

ilar to the special quasirandom structures (SQS) approach for amorphous structures [41]. If the missed substitutional patterns are of concern, it would also be possible to apply another heuristic method, such as a genetic algorithm using the same objective function, in a subsequent stage.

IV. CONCLUSION

In this study, we systematically examined the effectiveness of applying annealing methods to the pre-screening of a vast substitutional configuration space in solid solutions and disordered systems, using electrostatic energy, specifically Ewald energy, as the objective function. Specifically, the occupation states of substitutional sites were represented by 0/1 binary variables, and the Ewald energy was mapped onto an Ising-type Hamiltonian. This formulation allowed the search for low-Ewald-energy configurations to be treated as a combinatorial optimization problem. We implemented this formulation using simulated annealing (SA) and quantum annealing (QA). Through comparison with exhaustive search, we quantitatively evaluated the applicability of annealing methods in terms of the degree of search acceleration and whether substitutional structures giving the lowest energy could be captured without omission.

For the small-scale system CaYAlO₄, both SA and QA sampled almost no high-energy configurations and were confirmed to selectively extract structures in the low-energy region. For this system, SA captured the lowest-energy bin without omission with a speed-up of nearly 30 times relative to exhaustive search. QA also captured the lowest-energy bin without omission, while achieving a speed-up of more than 100 times. These results demonstrate that, when the problem size is sufficiently small, QA can also function as a practical high-speed search method.

In contrast, for the medium-scale system β -KSbF₄, SA showed a significant speed-up, although its performance de-

pended on the cooling schedule. In particular, linear cooling was found to achieve both a speed-up on the order of 200 times and suppression of omissions in the lowest-energy bin. Furthermore, even for the larger-scale Ba-doped SiAlON system, SA was able to capture the lowest-energy structures without omission with a speed-up of nearly 300 times. These results indicate that SA is an effective pre-screening method capable of extracting low-energy configuration groups within realistic computational resources, even for problems whose exhaustive evaluation is practically infeasible.

In contrast, for QA applied to β -KSbF₄, the lowest-energy bin could be captured by using a sufficiently long annealing time. However, the speed-up was limited in terms of computational time, and omissions occurred under short-annealing-time conditions. In this study, we quantitatively showed that chain breaks hinder the search for low-energy solutions, based on the correlation between the chain-break fraction and the average energy of the obtained solutions. These results suggest that, in current hardware implementations of QA, constraints associated with embedding can become a bottleneck in terms of both search performance and computational speed.

Overall, for Ewald-energy-based configuration search in mixed crystals, SA is currently the most robust and general-purpose high-speed approach. It was shown to achieve substantial improvements in computational efficiency even for large-scale systems while suppressing omissions. In contrast, although QA is promising for small-scale problems, improv-

ing implementation and embedding techniques, including the reduction of chain breaks, is an important issue for achieving stable performance in problems of realistic size.

The formulation used in this study can be implemented mechanically using publicly available libraries and is practical for incorporating rapid pre-screening based on Ewald energy into materials-design pipelines. By using the low-energy structures extracted from Ewald-energy screening as starting points and integrating them stepwise with first-principles calculations or other search methods, this framework can contribute to further acceleration of candidate-structure generation and property prediction for real materials systems.

ACKNOWLEDGMENTS

This work was supported by JST SPRING, Japan Grant Number JPMJSP202. The computations in this work have been performed using the facilities of Center for Advanced Scientific Computing at JAIST. K.H. is grateful for financial support from MEXT-KAKENHI, Japan (JP23K23438, JP24K07571, and JP25K01851) and JSPS Program for Forming Japan's Peak Research Universities (J-PEAKS; JPJS00420230006). R.M. is grateful for financial supports from MEXT-KAKENHI (22H051462, 24K01172, 24K07571A). T.I. appreciates the support from the JSPS KAKENHI Grant Number 24K17618 and JSPS Overseas Research Fellowships.

-
- [1] H. Kageyama, K. Hayashi, K. Maeda, J. P. Attfield, Z. Hiroi, J. M. Rondinelli, and K. R. Poeppelmeier, Expanding frontiers in materials chemistry and physics with multiple anions, *Nature Communications* **9**, 772 (2018).
- [2] K. Okhotnikov, T. Charpentier, and S. Cadars, Supercell program: a combinatorial structure-generation approach for the local-level modeling of atomic substitutions and partial occupancies in crystals, *Journal of Cheminformatics* **8**, 17 (2016).
- [3] G. I. Prayogo, A. Tirelli, K. Utimula, K. Hongo, R. Maezono, and K. Nakano, Shry: Application of canonical augmentation to the atomic substitution problem, *Journal of Chemical Information and Modeling* **62**, 2909 (2022), pMID: 35678099, <https://doi.org/10.1021/acs.jcim.2c00389>.
- [4] S. Gražulis, D. Chateigner, R. T. Downs, A. F. T. Yokochi, M. Quirós, L. Lutterotti, E. Manakova, J. Butkus, P. Moeck, and A. Le Bail, Crystallography Open Database – an open-access collection of crystal structures, *Journal of Applied Crystallography* **42**, 726 (2009).
- [5] K. Utimula, G. I. Prayogo, K. Nakano, K. Hongo, and R. Maezono, Stochastic estimations of the total number of classes for a clustering having extremely large samples to be included in the clustering engine, *Advanced Theory and Simulations* **4**, 2000301 (2021), <https://advanced.onlinelibrary.wiley.com/doi/pdf/10.1002/adts.202000301>.
- [6] X. Jin, S. Chen, and T. Li, Coexistence of two types of short-range order in Si–Ge–Sn medium-entropy alloys, *Communications Materials* **3**, 66 (2022).
- [7] K. Ichikawa, S. Ohuchi, K. Ueno, and T. Yokoyama, Accelerating optimal elemental configuration search in crystal using ising machine, *Phys. Rev. Res.* **6**, 033321 (2024).
- [8] S.-H. Jang, R. Jalem, and Y. Tateyama, Ewaldsolidsolution: A high-throughput application to quickly sample stable site arrangements for ionic solid solutions, *The Journal of Physical Chemistry A* **127**, 5734 (2023), pMID: 37381735, <https://doi.org/10.1021/acs.jpca.3c00076>.
- [9] C. J. Pickard, Real-space pairwise electrostatic summation in a uniform neutralizing background, *Phys. Rev. Mater.* **2**, 013806 (2018).
- [10] M. J. Rutter, Pseudopotential contributions to the quadrupole moment in charged periodic systems, *Phys. Rev. B* **107**, 075133 (2023).
- [11] M. G. Trefry, E. N. Maslen, and M. A. Spackman, Electrostatic, madeling and cohesive energies for solids, *Journal of Physics C: Solid State Physics* **20**, 19 (1987).
- [12] S. P. Ong, W. D. Richards, A. Jain, G. Hautier, M. Kocher, S. Cholia, D. Gunter, V. L. Chevrier, K. A. Persson, and G. Ceder, Python materials genomics (pymatgen): A robust, open-source python library for materials analysis, *Computational Materials Science* **68**, 314 (2013).
- [13] J. D. Gale and A. L. Rohl, The general utility lattice program (gulp), *Molecular Simulation* **29**, 291 (2003), <https://doi.org/10.1080/0892702031000104887>.
- [14] T. Binnering, Y.-Y. Ting, P. M. Kowalski, and M. H. Eikerling, Optimization of ionic configurations in battery materials by quantum annealing, *Phys. Rev. B* **110**, L180202 (2024).

- [15] S. Kirkpatrick, C. D. Gelatt, and M. P. Vecchi, Optimization by Simulated Annealing, *Science* **220**, 671 (1983), <https://www.science.org/doi/pdf/10.1126/science.220.4598.671>.
- [16] P. Song, Z. Hou, P. B. de Castro, K. Nakano, K. Hongo, Y. Takano, and R. Maezono, High-Tc Superconducting Hydrides Formed by LaH_{24} and YH_{24} Cage Structures as Basic Blocks, *Chemistry of Materials* **33**, 9501 (2021).
- [17] T. Alam, S. Qamar, A. Dixit, and M. Benaida, Genetic algorithm: Reviews, implementations, and applications, *International Journal of Engineering Pedagogy (iJEP)* **10**, pp. 57–77 (2020).
- [18] T. Ichibha, Y. Zhang, K. Hongo, R. Maezono, and F. A. Reberdo, Candidate structure for the H_2 -PRE phase of solid hydrogen, *Phys. Rev. B* **104**, 214111 (2021).
- [19] R. Eberhart and J. Kennedy, A new optimizer using particle swarm theory (1995) pp. 39–43, mHS'95. Proceedings of the Sixth International Symposium on Micro Machine and Human Science.
- [20] T. Yoshida, R. Maezono, and K. Hongo, Synergy of Binary Substitutions for Improving the Cycle Performance in LiNiO_2 Revealed by Ab Initio Materials Informatics, *ACS Omega* **5**, 13403 (2020).
- [21] B. Shahriari, K. Swersky, Z. Wang, R. P. Adams, and N. de Freitas, Taking the human out of the loop: A review of bayesian optimization, *Proceedings of the IEEE* **104**, 148 (2016).
- [22] T. Kadowaki and H. Nishimori, Quantum annealing in the transverse Ising model, *Phys. Rev. E* **58**, 5355 (1998).
- [23] R. Shannon, R. Oswald, J. Parise, B. Chai, P. Byszewski, A. Pajczkowska, and R. Sobolewski, Dielectric constants and crystal structures of CaYAlO_4 , CaNdAlO_4 , and SrLaAlO_4 , and deviations from the oxide additivity rule, *Journal of Solid State Chemistry* **98**, 90 (1992).
- [24] K. Yamada, Y. Ohnuki, H. Ohki, and T. Okuda, New anionic conductor KSbF_4 with fluorite structure, *Chemistry Letters* **28**, 627 (2003), <https://academic.oup.com/chemlett/article-pdf/28/7/627/56076277/cl.1999.627.pdf>.
- [25] S. Esmailzadeh, J. Grins, Z. Shen, M. Edén, and M. Thiaux, Study of Sialon S-phases $\text{M}_2\text{Al}_x\text{Si}_{12-x}\text{N}_{16-x}\text{O}_{2+x}$, $\text{M} = \text{Ba}$ and $\text{Ba}_{0.9}\text{Eu}_{0.1}$, by X-ray Single Crystal Diffraction, X-ray Powder Diffraction, and Solid-State Nuclear Magnetic Resonance, *Chemistry of Materials* **16**, 2113 (2004).
- [26] M. Xia, Y. Zhang, M. Li, Y. Zhong, S. Gu, N. Zhou, and Z. Zhou, High thermal stability and blue-violet emitting phosphor $\text{CaYAlO}_4:\text{Ti}^{4+}$ with enhanced emission by Ca^{2+} vacancies, *Journal of Rare Earths* **38**, 227 (2020).
- [27] Y. Liu, Y. Wang, M. Wang, H. Shen, C. Huang, X. Wang, J. Gao, and C. Tu, Structure and spectral properties of Dy^{3+} doped CaYAlO_4 single crystal, *Scientific Reports* **13**, 6066 (2023).
- [28] R. Hisasue, T. Saquai, T. Ichibha, Y. Fujii, A. Yamashita, K. Hongo, R. Maezono, K. Tadanaga, and A. Miura, Kinetic effects of ball-milling precursors on the synthesis pathway of KSbF_4 , *Ceramics International* **51**, 33653 (2025).
- [29] C. Duan, W. Otten, A. Delsing, and H. Hintzen, Photoluminescence properties of Eu^{2+} -activated sialon S-phase $\text{BaAlSi}_5\text{O}_2\text{N}_7$, *Journal of Alloys and Compounds* **461**, 454 (2008).
- [30] C. C. McGeoch and P. Farré, The d-wave advantage system: An overview technical report (2020).
- [31] D-Wave Systems, D-Wave Ocean SDK (2024).
- [32] W. Vinci, T. Albash, G. Paz-Silva, I. Hen, and D. A. Lidar, Quantum annealing correction with minor embedding, *Phys. Rev. A* **92**, 042310 (2015).
- [33] E. Grant and T. S. Humble, Benchmarking embedded chain breaking in quantum annealing*, *Quantum Science and Technology* **7**, 025029 (2022).
- [34] C. Roch, D. Ratke, J. Nüßlein, T. Gabor, and S. Feld, The effect of penalty factors of constrained hamiltonians on the eigenspectrum in quantum annealing, *ACM Transactions on Quantum Computing* **4**, 10.1145/3577202 (2023).
- [35] D. Willsch, M. Willsch, C. D. Gonzalez Calaza, F. Jin, H. De Raedt, M. Svensson, and K. Michielsen, Benchmarking advantage and d-wave 2000q quantum annealers with exact cover problems, *Quantum Information Processing* **21**, 141 (2022).
- [36] C. S. Pedamallu and L. Ozdamar, Investigating a hybrid simulated annealing and local search algorithm for constrained optimization, *European Journal of Operational Research* **185**, 1230 (2008).
- [37] F. A. Quinton, P. A. S. Myhr, M. Barani, P. Crespo del Granado, and H. Zhang, Quantum annealing applications, challenges and limitations for optimisation problems compared to classical solvers, *Scientific Reports* **15**, 12733 (2025).
- [38] M. Zaman, K. Tanahashi, and S. Tanaka, Pyqubo: Python library for mapping combinatorial optimization problems to qubo form, *IEEE Transactions on Computers* **71**, 838 (2022).
- [39] K. Hukushima and K. Nemoto, Exchange monte carlo method and application to spin glass simulations, *Journal of the Physical Society of Japan* **65**, 1604 (1996), <https://doi.org/10.1143/JPSJ.65.1604>.
- [40] C. Carugno, M. Ferrari Dacrema, and P. Cremonesi, Evaluating the job shop scheduling problem on a d-wave quantum annealer, *Scientific Reports* **12**, 6539 (2022).
- [41] A. Zunger, S.-H. Wei, L. G. Ferreira, and J. E. Bernard, Special quasirandom structures, *Phys. Rev. Lett.* **65**, 353 (1990).